Nanoscale

PAPER

View Article Online
View Journal | View Issue

Cite this: *Nanoscale*, 2022, **14**, 16536

Water structure, dynamics and reactivity on a TiO_2-nanoparticle surface: new insights from *ab initio* molecular dynamics†

Fredrik Grote and Alexander P. Lyubartsev *

Water structure, dynamics and reactivity at the surface of a small TiO_2-nanoparticle fully immersed in water was investigated by an *ab initio* molecular dynamics simulation. Several modes of water binding were identified by assigning each atom to an atom type, representing a distinct chemical environment in the *ab initio* ensemble, and then computing radial distribution functions between the atom types. Surface reactivity was investigated by monitoring how populations of atom types change during the simulation. In order to acquire further insight, electron densities for a set of representative system snapshots were analyzed using an atoms-in-molecules approach. Our results reveal that water dissociation, where a water molecule splits at a bridging oxygen site to form a hydroxyl group and a protonated oxygen bridge, can occur by a mechanism involving transfer of a proton over several water molecules. The hydroxyl group and protonated oxygen bridge formed in the process persist (on a 10 ps time scale) and the hydroxyl group undergoes exchange using a mechanism similar to the one responsible for water dissociation. Rotational and translational dynamics of water molecules around the nanoparticle were analyzed in terms of reorientational time correlation functions and mean square displacement. While reorientation of water O–H vectors decreases quickly in the proximity of the nanoparticle surface, translational diffusion slows down more gradually. Our results give new insight into water structure, dynamics and reactivity on TiO_2-nanoparticle surfaces and suggest that water dissociation on curved TiO_2-nanoparticle surfaces can occur *via* more complex mechanisms than those previously identified for flat defect-free surfaces.

Received 29th April 2022,
Accepted 30th September 2022

DOI: 10.1039/d2nr02354g

rsc.li/nanoscale

1 Introduction

Nanomaterials are nowadays used in an endless line of applications due to their unique physicochemical properties originating in the large surface area to bulk ratio, which makes them more reactive and having a higher adsorption capability when compared to their bulk counterparts.[1] One of the most widely used nanomaterials is TiO_2-nanoparticles.[2] TiO_2 exists in three polymorphic forms: rutile, anatase and brookite, with each one having different crystal structures. Rutile is the most thermodynamically stable form of TiO_2 as a bulk material but on the nanoscale, contributions from surface energy become important, which favours anatase. While the most stable shape of nanoparticles can be obtained, in theory, by a Wulff construction, TEM-micrographs show that real materials contain nanoparticles having different sizes, shapes[3] and surface facets.[4] Any realistic sample of TiO_2-nanoparticles contains a distribution of these facets and particle sizes, which can be sensitive to synthesis conditions. These features together with several others including the presence of surface defects, *e.g.* oxygen vacancies and step dislocations, have important consequences for properties of nanoparticles, and determine their potential use in various applications. For example, their photocatalytic properties have led to applications as coatings in self-cleaning materials.[5] Furthermore, the interaction of these materials with light make them useful as pigments as well as components in sunscreens.[6] TiO_2-nanoparticles are also important components in solar cells[7] and other energy applications, *e.g.* Li-ion batteries[8] and hydrogen production by water splitting.[9]

Recently, properties of nanoclusters, that is small nanoparticles under 2 nm in size, have become a hot topic of research due to the possibility of controlling a nanocluster structure at up to atomistic resolutions.[10] The photocatalytic efficiency of TiO_2 can be improved by nanostructuring where the size and shape of nanoclusters are controlled in order to optimize their catalytic properties.[11–13] Here, it is important to

Department of Materials and Environmental Chemistry, Stockholm University, Svante Arrhenius väg 16 C, 106 91 Stockholm, Sweden.
E-mail: alexander.lyubartsev@mmk.su.se

†Electronic supplementary information (ESI) available: Supplementary method details and supplementary figures (.pdf). See DOI: https://doi.org/10.1039/d2nr02354g

better understand the reactivity of small TiO_2-clusters with well-defined structures. Despite the significant progress in nanotechnology during the last decades, developing effective and green catalysts for energy applications and reducing the hazards of nanoparticles to humans and the environment remain central challenges for nanoscience. Since many of these processes take place in aqueous media, a detailed understanding of nanoparticle–water interactions is essential. Here, water dissociation and proton transfers modifying the nanoparticle surface and its interaction with the environment play an important role.

Experimentally, water reactivity on TiO_2-surfaces has been studied using X-ray photoelectron spectroscopy[14] (XPS) and X-ray absorption spectroscopy[15] (XAS), which have provided valuable insights into electronic structures and adsorption thermodynamics. The TiO_2–water interface has also been studied using nuclear magnetic resonance (NMR) spectroscopy[16] providing information about the structure and mobility of water around TiO_2-nanoparticles. These results have suggested that water molecules are organized in layers where the mobility of water molecules decreases with their proximity to the nanoparticle surface. Furthermore, Wang *et al.*[17] have conducted *in situ* molecular beam scattering STM studies, which provided a detailed picture of the energetics governing water dissociation on the rutile (110) surface. Their results provide evidence of water dissociation at bridging oxygen sites (2-coordinated oxygen atoms) leading to the formation of protonated oxygen bridges and hydroxyl groups. They reported that the energy difference between molecularly adsorbed water and dissociated water is on the order of k_BT at room temperature and that the energy barrier for dissociation is roughly $10k_BT$. This suggests that water dissociation on this surface occurs even at ambient conditions.

TiO_2–water interactions have also been studied using computational techniques, including density functional theory (DFT),[18] which emphasize the role of the local surface structure, in particular structural defects including step edges and oxygen vacancies. Classical molecular dynamics (MD) simulations, using standard molecular-mechanical force fields, have provided additional insights into water structures and dynamics at TiO_2-surfaces.[19–22] These simulations are, however, limited by the quality of force fields describing atomic interactions, which do not allow for the breaking or formation of chemical bonds as well as the absence of polarizability due to the use of a fixed point charge representation of the charge distribution. Huang *et al.* has partially resolved the first of these problems by carrying out MD simulations of TiO_2 and water using a reactive force field[23] allowing chemical bonds to break and form. Although this approach is very attractive from a computational point of view, it is also highly dependent on the parametrization of the interaction potential. Also, proton transfer reactions at the anatase (101) aqueous interface were probed by MD simulations with an *ab initio* trained neural network model.[24] With the continual increase of computer power, *ab initio* molecular dynamics simulations[25] (AIMD) have gained popularity. Here, the force acting on each atom is obtained by solving the electronic structure problem at each MD step making it possible for chemical bonds to break and form and allowing the electronic cloud to deform in response to electric fields. In practice, however, this approach is currently limited to system sizes of up to 1000 atoms and a 10 ps time scale. The interaction between water and a number of flat defect-free TiO_2-surfaces has been studied using AIMD simulations.[26] These simulations gave important mechanistic insights into water structure and water dissociation on the investigated surfaces showing that water molecules split *via* a number of mechanisms involving one or two water molecules.

It can be suggested that a real nanoparticle represents some mixture of different surfaces with various defects, *i.e.* at edges between the surfaces. Defects can be associated with certain effects that are not captured by the planar defect-free geometry of slab systems. On a curved surface, water molecules can arrange in ways that are not possible on a planar surface due to the absence of curvature. Surface atoms at the place of defects are often more under-coordinated compared to atoms at an ideally planar surface. Furthermore, reactive events often take place on edges, which are not present in a periodically repeated defect-free slab. Attempts to consider these effects were made by *ab initio* simulations of smaller TiO_2-clusters in the presence of water molecules, focusing on wetting thermodynamics.[27] However, the size of these systems was rather limited (nanoparticle diameter of ~1 nm), and the number of water molecules $n_{H_2O} \leq 30$ corresponded to no more than one layer of water at the nanoparticle surface. To access effects of an irregular surface on water hydration, in this work we have carried out an AIMD simulation of a larger nanoparticle (~1.5 nm) fully immersed in water in order to gain detailed atomistic insights into water structure, dynamics and reactivity on TiO_2-surfaces that are different from the planar defect-free systems that have been studied previously. Recently the TiO_2–water interface has also attracted interest in the context of the decoupling of translational and rotational diffusion similar to the anomalies that have been observed in supercooled water.[28] This also makes these systems interesting from a theoretical point of view. We have therefore carried out an extensive analysis of translational and reorientational dynamics of water molecules as a function of the distance to the nanoparticle surface. The next section, "Methods and models", describes details of the simulated system and the analysis of the obtained trajectory and electron density. In the "Results and discussion", we present and discuss the results from this analysis. The last section, "Conclusion", provides our concluding remarks.

2 Methods and models

The simulated system was generated starting from the anatase crystal structure replicating the unit cell in *x*-, *y*- and *z*-dimensions. A nanoparticle was constructed by removing all atoms outside a sphere of radius 8.5 Å taking the origin of the sphere

to coincide with the origin of the unit cell and then removing all undercoordinated atoms (Ti with 3 or less bound oxygens, and oxygens bound to a single Ti atom) from the surface. The obtained nanoparticle contains 53 titanium atoms and 104 oxygen atoms and has a maximum diameter of about 16 Å. It was solvated by 426 water molecules in a 3D periodic cell of size 24.3 Å, giving a water layer of roughly 10 Å between the nanoparticle and its periodic image. The whole system contains 1435 atoms (see Fig. 1a), and was first simulated at constant temperature and pressure using a classical force field[29] for 50 ns in order to obtain a realistic density. The box volume was then fixed and a Born–Oppenheimer *ab initio* molecular dynamics simulation (AIMD) was started using CP2K software.[30] Electronic structure calculations were performed using density functional theory (DFT) within the Gaussian and plane wave method[31] (GPW) as implemented in the QUICKSTEP module.[32] Exchange and correlation were described on the generalized gradient (GGA) level using the functional developed by Becke–Lee–Yang–Parr.[33,34] Since GGA functionals do not accurately describe the long-range dispersion interaction, we also included the DFT-D3 dispersion correction by Grimme.[35] The MOLOPT-DZVP basis set[36] was used together with GTH pseudopotentials[37] describing core electrons. The same combination of basis set and pseudopotentials has previously been used for similar systems.[26] A 200 Ry plane wave cutoff was used and the relative cutoff was set to 30 Ry with a four-level multigrid; further details for this choice are provided in the ESI, Section S1, Fig. S1 and S2.† The system was simulated for 49 ps in an NVT ensemble using a time step of 0.5 fs. The temperature was held constant at 300 K using the thermostat of Bussi, Donadio and Parrinello[38] with a time constant of 0.1 ps. All simulations in this work used periodic boundary conditions in *x*-, *y*-, and *z*-dimensions.

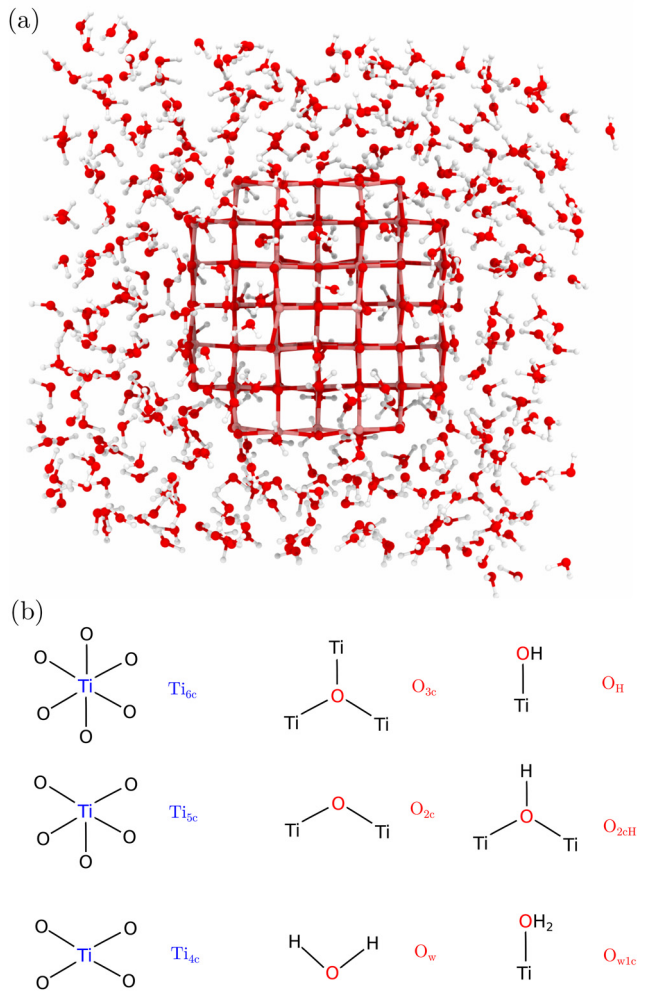

Fig. 1 (a) Visualization showing the simulated system consisting of an anatase nanoparticle solvated in water where oxygen atoms are shown in red, hydrogen atoms in white and titanium in brown and (b) atom types for Ti and O atoms.

Equilibration was monitored by following how temperature, potential energy, root mean square displacement (RMSD) of the nanoparticle atoms, and radial distribution functions (RDF) were changing as functions of time (Section S2, Fig. S3 and S6†). As shown in the ESI (Fig. S3†), temperature and potential energy reached stable levels within 1 ps. The RMSD of the nanoparticle atoms (Fig. S4†), obtained with respect to the original crystalline structure for both surface and interior atoms, shows a slightly increasing trend but remains low, indicating that no structural transformation occurred, and the structure remains close to the anatase phase. Similar conclusions were made from previous *ab initio* simulations of weakly hydrated TiO_2-nanoparticles.[27] RDF computed between Ti and O atoms showed a stable shape after 1 ps of the simulations (Fig. S5†). We also computed RDF between water hydrogen and surface oxygen atoms (O_{2c}) during different time windows (Fig. S6†), which confirmed that the structure of the interface reached equilibrium. This short equilibration time can be explained by the fact that the starting structure of the AIMD simulation was obtained as a result of a 50 ns simulation with a classical force field, which provided an almost equilibrium structure needing only a short time to adjust to *ab initio* interactions. In the analysis of the simulation, we excluded the first 3 ps of the trajectory.

3 Results and discussion

3.1 Atom types

In order to discuss the structure and reactivity in the simulated system it is convenient to group atoms into atom types representing distinct chemical environments. It is natural to distinguish atoms based on their local coordination. In TiO_2, titanium atoms can be 6-, 5- or 4-coordinated to oxygens. Oxygen atoms in the bulk of the material are 3-coordinated while surface oxygens are 2-coordinated to titanium (*i.e.*, they are bridging oxygens). Furthermore, water molecules can adsorb to titanium atoms on the surface forming molecularly adsorbed water. Dissociation of water molecules on the surface leads also to the formation of hydroxyl groups and protonated oxygen bridges. These coordination environments form the

collection of possible atom types that is shown in Fig. 1b, together with assigned names used later on in the text.

Each atom in the system can be mapped onto one of these atom types at every point during the simulation by determining the coordination number of atoms by counting other atoms that fall within a certain cut-off radius. However, the atom types determined by such geometrical criteria will frequently change due to fast bond oscillations and will not always represent actual chemical transformations from one type to another. In order for the change in atom types to reflect the change of local environment due to reactive events, we must average out these fast bond vibrations. For this reason, we assign atom types in 100 fs windows to determine coordination numbers of atoms by averaging the number of neighboring atoms found within a sphere of radius R, which represents the maximal distance where atoms can still be considered as bonded to each other, here taken to be the first minimum of the respective RDF. For Ti–O we use R = 3.0 Å and for O–H we take R = 1.3 Å. Populations of atom types obtained using this algorithm for the start configuration (generated by a simulation with the classical force field) and averaged over the whole trajectory of the AIMD simulation are presented in Table 1. Note that the original (non-hydrated) nanoparticle contained 21, 12 and 20 of Ti6c, Ti5c and Ti4c atoms, respectively, but upon hydration and adsorption of water molecules during a classical MD simulation the number of 4- and 5-coordinated Ti atoms was greatly reduced, and in particular no 4-coordinated Ti atoms remained. We observed that during almost 50 ps of the AIMD simulation only small changes in the populations take place: a small increase of Ti5c (5-coordinated) Ti atoms, and the appearance of small amounts of O_H (hydroxyl) and O_{2cH} (protonated bridge) types of oxygen atoms due to the splitting of water molecules (discussed in more detail below). This situation is different from that of the previous AIMD simulation of a TiO_2 anatase nanoparticle at low hydration where about 30% of water molecules were split to form surface hydroxyl groups,[27] and also from simulations of plain anatase TiO_2 slabs, which showed no water splitting or reactivity at some surfaces ((100) and (101)) while there was a high level of reactivity at the (001) surface where hydroxyl groups were formed at about one-third of all surface Ti sites.[26] Experimentally, high numbers of OH^- groups were found on the anatase (101) surface at low hydration[39] while sum frequency generation spectrum measurements and AIMD simulations indicated a stable bilayer of intact water molecules on the anatase (101) surface at full hydration.[40]

In order to feel further confidence that this choice of atom types is physically motivated, we carried out an atoms-in-molecules analysis where a set of snapshots from the trajectory were extracted and from their electron densities net atomic charges were computed using the DDEC6 method.[41] The result presented in Table 1 shows that the difference of net atomic charges between atom types is larger or about the same as the spread within the types, which is also seen in the distributions of net atomic charges presented in Fig. S7 in Section S3 of the ESI.† Furthermore, the charges computed for the nanoparticle are very similar to previously computed net charges for a planar surface of the same atom types. This suggests that the atom types to which we have assigned atoms represent distinct chemical environments, and they are transferable over different types of surfaces. These atom types can be useful for discussions of surface chemistry and other processes taking place on TiO_2-nanoparticle surfaces including biomolecular adsorption and catalysis. They also form a natural choice of atom types for use in classical MD simulations, which is needed in order to simulate longer lengths and time scales. In addition, the distribution of atom types presented here can provide important guidance for setting up starting configurations for such simulations.

3.2 Water density distribution and radial distribution functions

In order to characterize the structure of the TiO_2–water interface we computed the density distribution of water molecules located in shells between R and $R + dr$ where R is the minimum distance between the water oxygen atom and any atom in the nanoparticle, and dr = 0.1 Å. The obtained distribution, shown in Fig. 2, shows two sharp peaks in the range of

Table 1 Net atomic charges for the nanoparticle obtained in this work (q_{NP}) and anatase (101) surface as reported in ref. 26 (q_{slab}) for different atom types identified in the AIMD ensemble (average charge ± standard deviation), with atom type populations at the start (N_{start}) of the simulation and their averages over the trajectory (N_{mean}) of the simulation

Atom type	q_{NP} (e)	q_{slab} (e)	N_{start}	N_{mean}
Ti_{6c}	2.16 ± 0.05	—	50	48.69
Ti_{5c}	2.08 ± 0.04	2.2	3	4.31
O_{3c}	−1.15 ± 0.03	—	58	58.00
O_{2c}	−1.06 ± 0.03	−1.0	46	45.53
O_w	−0.75 ± 0.03	−0.753	377	378.30
O_{w1c}	−0.81 ± 0.03	—	49	47.23
O_H	−0.91 ± 0.03	—	0	0.46
O_{2cH}	−1.00 ± 0.02	—	0	0.47
H	0.38 ± 0.02	0.43	852	852.00

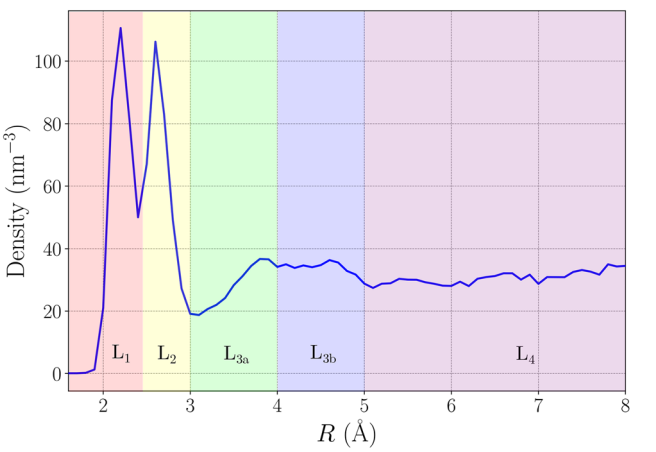

Fig. 2 Water density distribution as a function of distance from the nanoparticle surface with water layers L_1, L_2, L_{3a}, L_{3b} and L_4.

2–3 Å followed by a less pronounced broader maximum centered just above 4 Å and a bulk region beyond 5 Å. This is consistent with distributions obtained in previous AIMD studies for hydrated anatase slab systems, which have described the interface in terms of water layers labeled L_1–L_4.[26,28] Layer L_1 (R < 2.5 Å) is assigned to molecularly adsorbed water (water oxygen bonded to titanium) and L_2 (2.5 Å < R < 3.0 Å) corresponds to water hydrogen bonded to a bridge oxygen of the nanoparticle. Notably, the density profile obtained here for a nanoparticle is most similar to the profile computed previously by AIMD simulations using the same calculation settings for the anatase (101) plane surface, but differ in some details from other surfaces.[26] As reported for the slab system, we found the density of the first maximum is about three times higher than the average value. Interestingly, we found that the second maximum in our system is almost as high as the first, while being more reduced for the slab, suggesting that the water molecules are found in a more densely packed arrangement in the L_2-layer of the nanoparticle compared to the slab. A third water layer is centered just above 4 Å. This broad peak consists of two maxima that have been labeled L_{3a} (3.0 Å < R < 4.0 Å) and L_{3b} (4.0 Å < R < 5.0 Å). Beyond this distance the density is stable at around 30 water molecules per cubic nanometer, corresponding to the bulk density of water, and this region is referred to as L_4 (R < 5.0 Å).

While the water density distribution gives an overall picture of the structure of the TiO_2–water interface, a more detailed description can be obtained by analyzing correlations between individual atom types. RDFs are important functions for characterization of structure, in particular for systems where there is no long-range order and where only local correlations occur. In order to obtain detailed structural information about the simulated system, we calculated RDFs between the atom types defined in the previous section. Of particular interest are RDFs between atom types belonging to the nanoparticle and water since these contain valuable information about the structure of the TiO_2–water interface. Fig. 3 shows RDFs between different oxygen and hydrogen atom types. The RDF between oxygen in bulk water (O_w type) and hydrogen, as shown in Fig. 3(a), has three peaks typical for O–H RDF in pure water. A high and narrow peak appears just above 1 Å and corresponds to the covalent O–H bond, with the broader one, centered at just below 2 Å, being assigned to the hydrogen of a hydrogen-bonded water molecule, while the third peak at roughly 3.5 Å corresponds to another hydrogen bonding of that molecule to a second solvation shell. The RDF in Fig. 3(b) between oxygen in molecularly adsorbed water (O_{wlc} type) and hydrogen atoms shows 3 peaks in similar positions but of different magnitudes. In particular, the peak at roughly 2 Å, corresponding to hydrogen bonding, is significantly reduced due to coordination of oxygen to the nanoparticle surface, which hinders hydrogen bonding to another water molecule. Fig. 3(c) shows the RDF between bridging (2-coordinated) oxygen atoms and hydrogen. This RDF has a well-expressed hydrogen bond peak just below 2 Å and a second broader peak at about 2.5 Å. It can be noted that correlations between bridging oxygens and hydrogen persist for longer when compared with those between oxygen atoms in bulk water and hydrogen. This can be attributed to an ordering effect of the rigid nanoparticle structure. Fig. 3(d) shows the RDF between 3-coordinated oxygen atoms and hydrogen. In this graph the characteristic peak due to hydrogen bonding is completely absent and the RDF has complex structure beyond 3 Å since O_{3c} atoms are found throughout the interior of the nanoparticle at different distances from the surface. This shows that only bridging oxygen atoms are involved in hydrogen bonding while 3-coordinated oxygen atoms are either found in the interior of the nanoparticle or in buried surface sites where formation of hydrogen bonds is not possible. Consistently, RDFs between oxygen atom types O_{3c}–O_H and O_{2c}–O_H presented in Fig. S8 in Section S4 of the ESI† show a pronounced hydrogen bond peak at about 3 Å for O_{2c}, which is absent for O_{3c}. In Fig. 3(e), the RDF between oxygen as a protonated bridging oxygen (O_{2cH}) and hydrogen is shown. This RDF is essentially identical to that for the O_w–H bond but is noisier since there is only one atom belonging to atom type O_{2cH}. Fig. 3(f) shows the RDF between oxygen in a hydroxyl group (O_H) and hydrogen. This RDF shows that the highest hydrogen bond peak is attributed to strong hydrogen bonding between the hydroxyl oxygen and a hydrogen in water.

Fig. S9 in Section S4 of the ESI† show RDFs between titanium atom types and the oxygen atom of water. The RDFs for Ti_{6c}–O_{wlc} and Ti_{5c}–O_{wlc} bonds are presented in Fig. S9(a) and S9(b)†. These RDFs have a high peak just above 2 Å corresponding to the bond between titanium atoms and oxygen atoms in molecularly adsorbed water molecules. The peaks occurring at longer distances correspond to titanium atoms and oxygen in molecularly adsorbed water separated by several bonds. Fig. S9(c) and S9(d)† show the corresponding RDFs between titanium atom types and oxygen atoms in water molecules in the bulk nanoparticle. Here the first maximum occurs at 4 Å since water molecules located closer than this distance are those which are adsorbed to the surface. A third shell of water molecules gives rise to a maximum at roughly 7 Å showing that structural correlations in the water surrounding the nanoparticle persist out to at least this distance.

RDFs between titanium atom and oxygen atom types in the nanoparticle are shown in Fig. S10 in Section S4 of the ESI.† These RDFs all have a sharp peak at about 2 Å corresponding to the bond between titanium and oxygen. At roughly 4 Å a broader peak occurs, which is due to titanium–oxygen neighbors that are separated by more than one bond.

The RDFs presented here give a detailed insight into the structure of the TiO_2-nanoparticle and the TiO_2–water interface and can be important target data in parametrization of classical force fields for these systems.

3.3 Water dissociation and hydroxyl exchange

Characterizing the dynamics and chemical transformations that water molecules undergo in the near-surface region is of significant importance for several processes taking place at the interface. Chemical transformations on the TiO_2-surface were

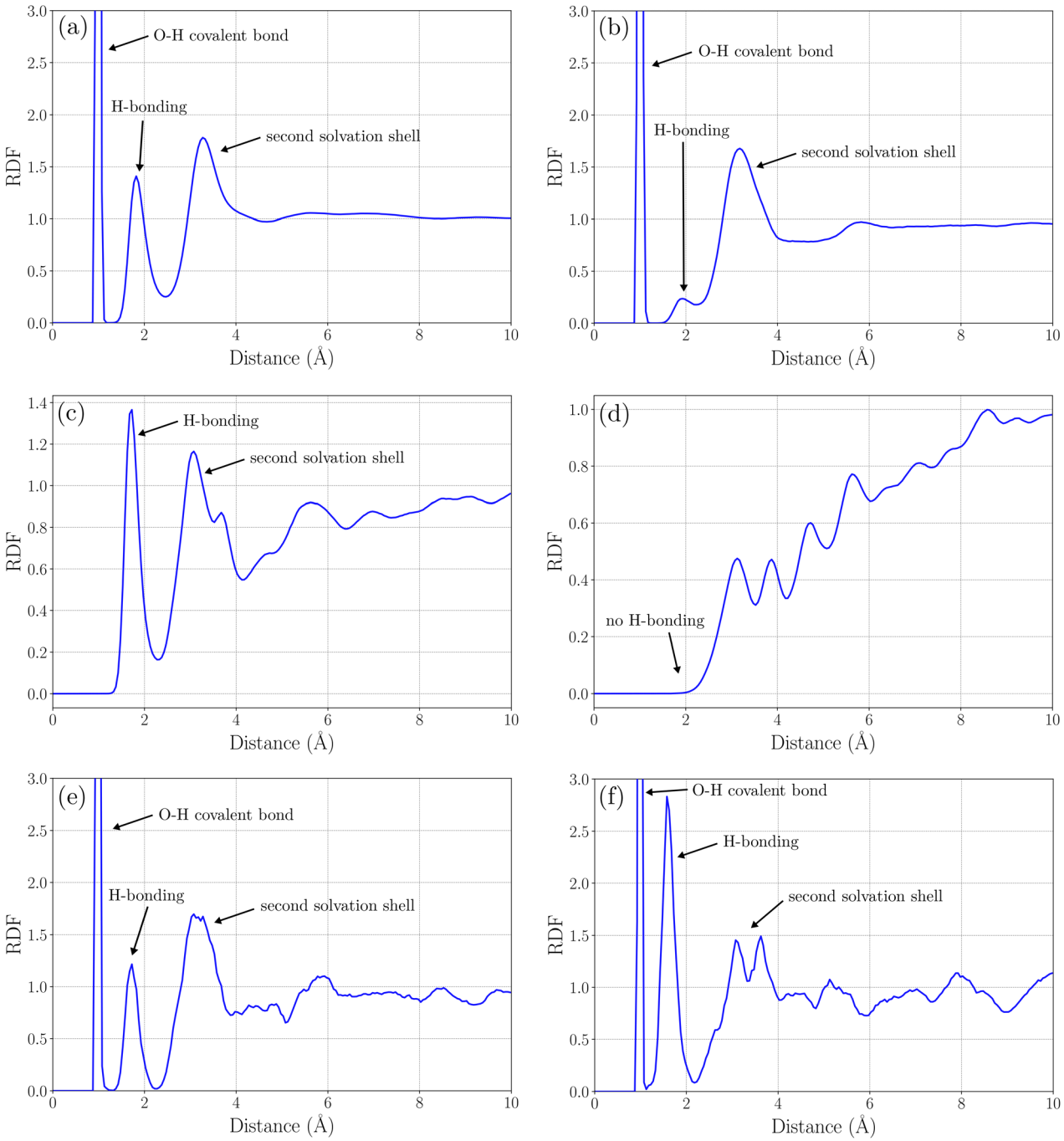

Fig. 3 Oxygen–hydrogen RDFs between atom types (a) O_w–H, (b) O_{wlc}–H, (c) O_{2c}–H, (d) O_{3c}–H, (e) O_{2cH}–H, and (f) O_H–H.

identified by monitoring how the populations of atom types change during the simulation. We found that the O_{2c}- and the O_w-population decreased by 1 after roughly 30 ps following the start of the simulation, while the O_{2cH}- and the O_H-population increased by 1 suggesting that water dissociates to form a hydroxyl group and a protonated oxygen bridge. After being formed these groups remain for the rest of the simulation. However, it is observed that the formed hydroxyl group undergoes further exchange with water molecules in the solution. Here we give a detailed account of the observed reactions.

As illustrated in Fig. 4a these events take place on an edge/corner of the nanoparticle, which is shown in close up in Fig. 4b together with three coordinated water molecules that play key roles in the set of reactions that lead to the splitting of a water molecule. We now turn to a more detailed analysis of how water dissociates on the surface. The atoms involved in the reaction are shown in Fig. 4c where we have also marked two distances that will be used in our discussion. Fig. 5 shows the O_{75}–H_{948} and O_{430}–H_{431} distances as functions of time. In order to illustrate the mechanism by which water dissociation

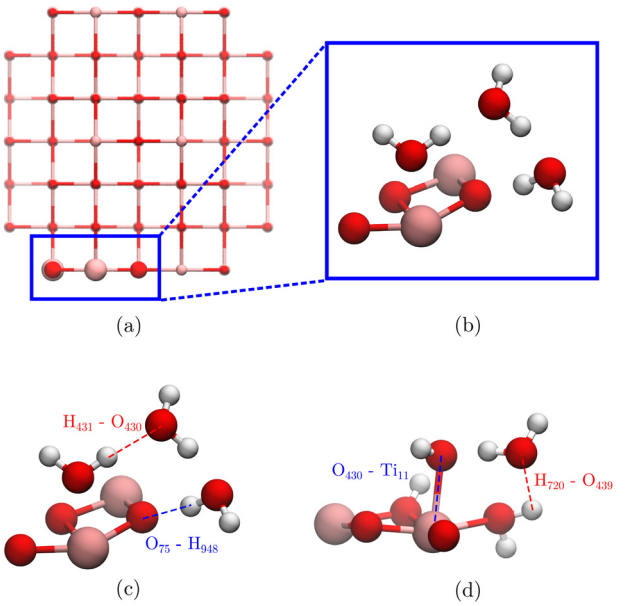

Fig. 4 Visualization showing (a) a region on the nanoparticle where water dissociation occurs, (b) a reactive region in close-up and water molecules involved in the dissociation mechanism, (c) distances used in the analysis of water dissociation, and (d) distances used in the analysis of hydroxyl group exchange.

occurs, a number of snapshots have been extracted along the reaction pathway. In snapshot 1, three water molecules are arranged in a hydrogen-bonded constellation around a bridging oxygen atom. The water molecule closest to the oxygen bridge then shares one of its protons with the bridging oxygen, as shown in snapshot 2, forming the configuration in snapshot 3. This structure is not stable, and the proton is quickly captured back by the water molecule (snapshot 4). However, the configuration in snapshot 3 is then formed again, as shown in snapshot 5. Then a synchronous proton transfer over three water molecules occurs leading to the dissociation of a water molecule and the formation of a hydroxyl group and a protonated oxygen bridge. As illustrated in snapshot 6, a water molecule adsorbed to a Ti-atom donates a proton to a neighboring water molecule, which donates one of its proton to the water molecule at the oxygen bridge, which in turn donates one of its protons to the oxygen bridge and then diffuses out into the solution. This mechanism involves three water molecules, where one is bridge protonating (BP-water), the second is hydroxyl group forming (HF-water), and the third is proton mediating (PM-water) and transfers a proton between the BP- and the HF-water. This result suggests that water dissociation on curved TiO_2 surfaces can occur by mechanisms involving complex proton transfers over several molecules.

Although interatomic distances are easy to interpret and provide important information about breaking and formation of chemical bonds, it should be pointed out that the spatial proximity of two atoms does not unambiguously quantify the amount of covalent interaction between them. For this reason, we have repeated the analysis presented here using bond orders, computed from the electron density of the snapshots in Fig. 5, instead of interatomic distances. Bond orders

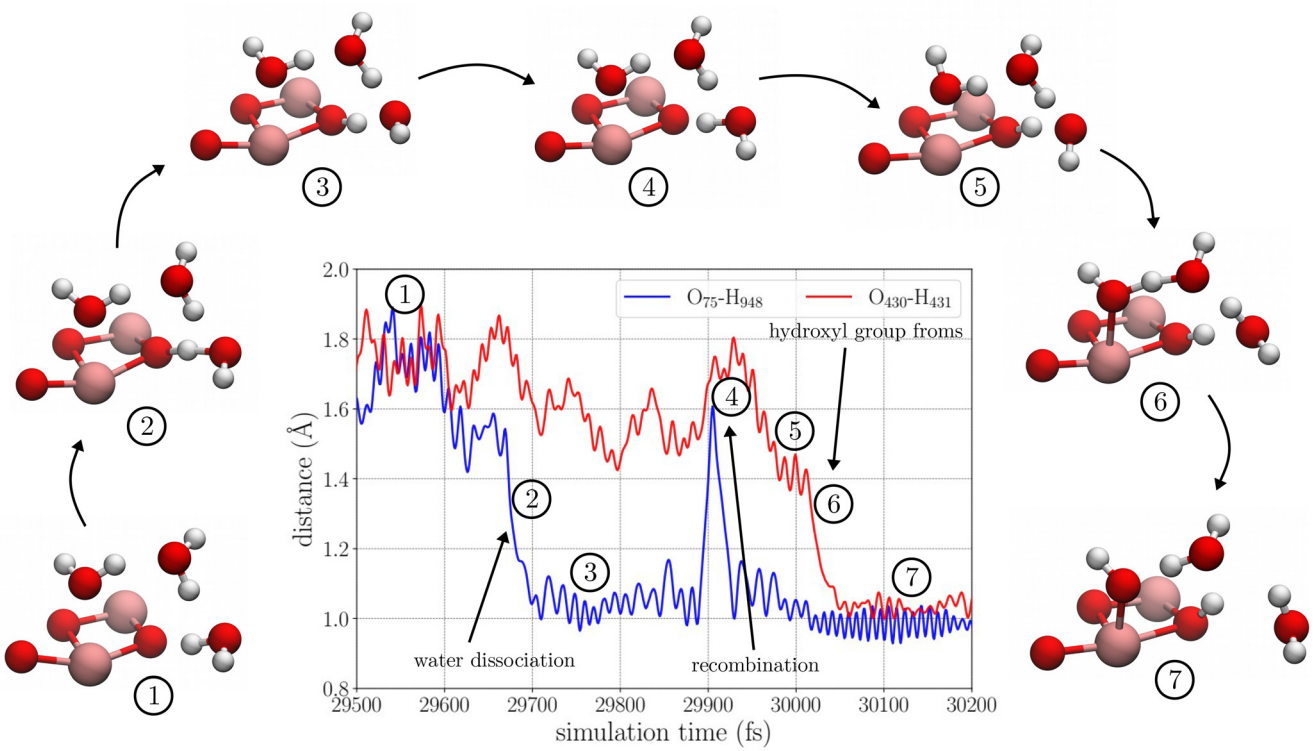

Fig. 5 Distances between atoms O_{75}–H_{948} and O_{430}–H_{431} as a function of time during water dissociation.

provide information about the amount of shared electron density between atoms due to 'dressed exchange' and are considered good indicators of the extent of covalent interactions between atoms. In the ESI (ection S5, Fig. S11†), we show that the analysis using bond orders leads to the same results as the approach presented here.

In previous works,[42] proton transfer was described using two coordinates: (1) the donor–acceptor distance and (2) $\delta = R_{A-H} - R_{D-H}$, where R_{A-H} is the distance between the acceptor atom and the proton and R_{D-H} is the distance between the donor atom and the proton. In order to obtain further insight, we computed the distribution of these coordinates during water dissociation. The free energy profiles along δ for short and intermediate donor–acceptor distances have been reported to be symmetric double-well separated by a barrier. As the donor–acceptor distance decreases the barrier becomes smaller facilitating proton transfer between the donor and acceptor. This picture is consistent with the distribution shown in Fig. S12 in Section S6 of the ESI† being nearly symmetric about $\delta = 0$ with two maxima corresponding to the proton bonded to a donor and an acceptor, respectively. From this graph, it is also evident that the proton is transferred when the donor–acceptor distance is short, *i.e.*, 2.5–2.6 Å.

Another observed event involving the rearranging of chemical bonds was hydroxyl group exchange. We carried out a similar analysis of atomic distances, defined in Fig. 4d, as was done for the water dissociation. Fig. 6 shows the O_{430}–Ti_{11} and O_{439}–H_{720} distances as functions of time and a set of snapshots extracted along the reaction pathway. Snapshot 1 shows a configuration with a water molecule adsorbed to a Ti-atom with a hydroxyl group and between them there is a second water hydrogen-bonded to the hydroxyl group. Because of thermal fluctuations, the second water molecule can donate its proton to the hydroxyl group (see snapshot 2), and simultaneously accept a proton (as shown in snapshot 3) from the adsorbed water, which then forms a hydroxyl group. This results in the structure shown in snapshot 4 where the hydroxyl group has been exchanged. This suggests that hydroxyl group exchange can occur by a mechanism similar to the one presented for water dissociation. One water protonates the hydroxyl group, while another water mediates a proton from an adsorbed water molecule. Just as in the mechanism for water dissociation this requires several water molecules to come together in a specific arrangement where proton transfer occurs. This suggests that the local surface structure (*i.e.* curvature, edges and defects) is of considerable importance for the surface chemistry of these materials. Our results show that water dissociation on curved TiO_2-surfaces with edges can be more complex than water dissociation previously discovered for flat surfaces.

3.4 Water adsorption/desorption equilibrium

The L_1 layer in the density distribution contains molecularly adsorbed water (type O_{wlc}), *i.e.*, intact water molecules bonded to titanium. Previous AIMD simulations of plain slab systems have indicated that these water molecules are strongly bound

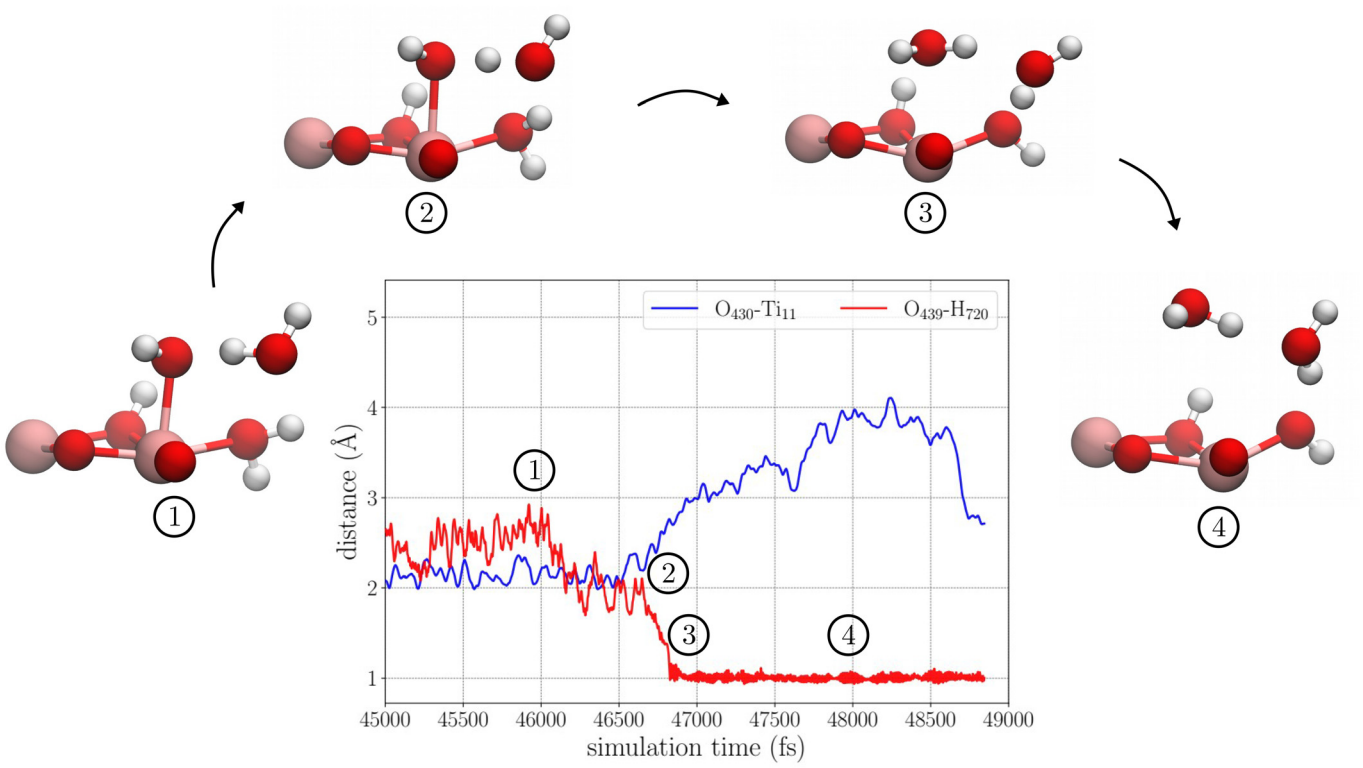

Fig. 6 Distances between atoms O_{75}–H_{948} and O_{430}–H_{431} as a function of time during hydroxyl group exchange.

to surface titanium atoms and do not interchange throughout whole simulations. In order to understand the behavior of molecularly adsorbed water in nanoparticle simulations, we analyzed how the number of atoms belonging to atom types Ti_{6c}, Ti_{5c}, O_w and O_{wlc} change as a function of time. The results (see Fig. S13a and b in Section S7 of the ESI†) show that changes between types Ti_{6c} and Ti_{5c} occur frequently and are associated with a corresponding change in populations of O_w and O_{wlc} attributed to the adsorption/desorption of water. Furthermore, we identified those titanium sites on the nanoparticle surface that can change between Ti_{6c} and Ti_{5c} types (see Fig. S13c in Section S7 of the ESI†), showing that water adsorption/desorption events occur on exposed titanium atoms located on edges and corners of the nanoparticle. These results indicate that water molecules on the nanoparticle surface undergo an adsorption/desorption equilibrium over a 10 ps time scale and highlight the importance of nanoparticle curvature, edges and local geometry for surface reactivity.

3.5 Water dynamics near the TiO_2 surface

Several previous studies, both experimental and theoretical, showed that the dynamics of water molecules is reduced as they come into proximity of the TiO_2 surface.[16,21,26] Interactions between water and the nanoparticle surface can be expected to slow down both the reorientational dynamics and diffusion of water molecules. Interestingly, recent studies have suggested a decoupling of rotational and translational diffusion for water molecules in the proximity of the nanoparticle surface where translational diffusion decreases while rotational diffusion is less affected.[28] In order to characterize how the dynamics of water is affected by its proximity to the nanoparticle surface, we analyze molecules located in layers L_1–L_4. The reorientational dynamics is characterized by the orientational time correlation function (TCF):

$$C(\tau) = \langle P_2[\hat{\mathbf{u}}(t) \cdot \hat{\mathbf{u}}(t+\tau)] \rangle \quad (1)$$

where $\hat{\mathbf{u}}(t)$ is a unit vector at a time origin t and $\hat{\mathbf{u}}(t + \tau)$ is the same vector at a later time $t + \tau$ where τ is a lag time, and $P_2(x) = \frac{3}{2}x^2 - \frac{1}{2}$ is the second order Legendre polynomial. Here $\hat{\mathbf{u}}$ was taken to be a unit vector along the O–H bond. The angle brackets in eqn (1) denote an average over all time origins t on the trajectory and all water molecules present within the considered region both at time t and $t + \tau$. Fig. 7a shows the obtained TCFs. While the decay of the TCF is similar for L_3 and L_4 ($R > 3$ Å) it is observed that the TCF decays significantly slower for L_2 and L_1 ($R < 3$ Å). This shows that the reorientational dynamics of water molecules is significantly decreased in the proximity of the TiO_2-surface. Fig. 7a also includes the total TCF where all water molecules in the system are included in the analysis. It is evident that the total TCF is dominated by the contribution from bulk water resulting in a fast decay. Interestingly, the reorientation of water O–H vectors is faster for L_1 than L_2. In order to gain further insight into the difference between water reorientation in layers L_1 and L_2 we computed the TCF for three orthogonal unit vectors in the water molecule $\hat{\mathbf{u}}_1$, $\hat{\mathbf{u}}_2$ and $\hat{\mathbf{u}}_3$ (see Fig. S14 in Section S8 of the ESI†). Here, $\hat{\mathbf{u}}_1$ bisects the HOH angle, $\hat{\mathbf{u}}_2$ is taken along the H–H separation and $\hat{\mathbf{u}}_3 = \hat{\mathbf{u}}_1 \times \hat{\mathbf{u}}_2$. The obtained time correlation functions show that reorientation of all three vectors $\hat{\mathbf{u}}_1$, $\hat{\mathbf{u}}_2$ and $\hat{\mathbf{u}}_3$ is faster in the L_1-layer compared to L_2.

In order to analyze water diffusion near the TiO_2 surface we computed mean square displacement (MSD) of water in layers L_1–L_4. MSD was computed for water oxygen atoms present in the region both at initial time t and later time $t + \tau$. The resulting MSD curves (see Fig. 7(b)) show that the mobility of water molecules is strongly reduced as they come into the proximity of the surface. In contrast to the reorientational dynamics, which decreases abruptly at $R = 3$ Å, it is observed that a decrease of translational diffusion starts at longer distances from the surface. Fig. 7(b) also shows the total MSD (computed over all water molecules), which increases faster than MSD-curves for $R = 2$–5 Å due to interlayer diffusion and a contribution from water molecules located at $R > 5$ Å. Diffusion coefficients were computed by fitting straight lines to the MSD plots presented in Fig. 7(b) in the range where the MSD is linear (4 ps $\leq \tau \leq$ 20 ps) according to eqn (2):

$$D = \lim_{\tau \to \infty} \frac{1}{4} \frac{d}{d\tau} \left\langle |\vec{r}(t+\tau) - \vec{r}(t)|^2 \right\rangle \quad (2)$$

where $\vec{r}(t)$ is the position of a water oxygen atom at time t and $\vec{r}(t+\tau)$ is the position of the atom at a later time $t + \tau$ with τ being the time lag. A plot of the diffusion coefficient as a function of distance from the nanoparticle is provided in Fig. S15 in Section S9 of the ESI.† This shows that the interaction between water and TiO_2 slows down diffusion of water molecules close to the nanoparticle surface and the most significant change occurs between 3 and 4 Å, which can be understood in that diffusion of water both in the first and second hydration layers is strongly affected by the surface. Similar (or even stronger) slowing down of water diffusion was observed previously for planar TiO_2 surfaces.[26]

We address further the question of a possible decoupling of translational and rotational diffusion. Fig. 7(c) shows the TCF of the water O–H vector as a function of the MSD taken over the same time. From this graph, one observes an indication of how far water molecules diffuse per rotation for each of the shells L_1–L_4, *i.e.*, a faster decay means that the molecule diffuses over a shorter distance per rotation. While the TCFs for L_3 and L_4 show a similar decay, it is observed that for L_2 TCF decreases more slowly and for L_1 it decreases more quickly. This means that the displacement per rotation in layer L_2 is larger than it is in L_3 and L_4, which in turn is larger than it is for L_1, thus supporting the decoupling of rotational and translational diffusion in the proximity of the nanoparticle surface.

The motion of water molecules changing hydration shell can also be characterized by survival probability, which is the probability that a water molecule initially residing inside a selected region (shell) remains inside that region after a given time, and is defined according to eqn (3):

$$P(\tau) = \left\langle \frac{N(t+\tau)}{N(t)} \right\rangle \quad (3)$$

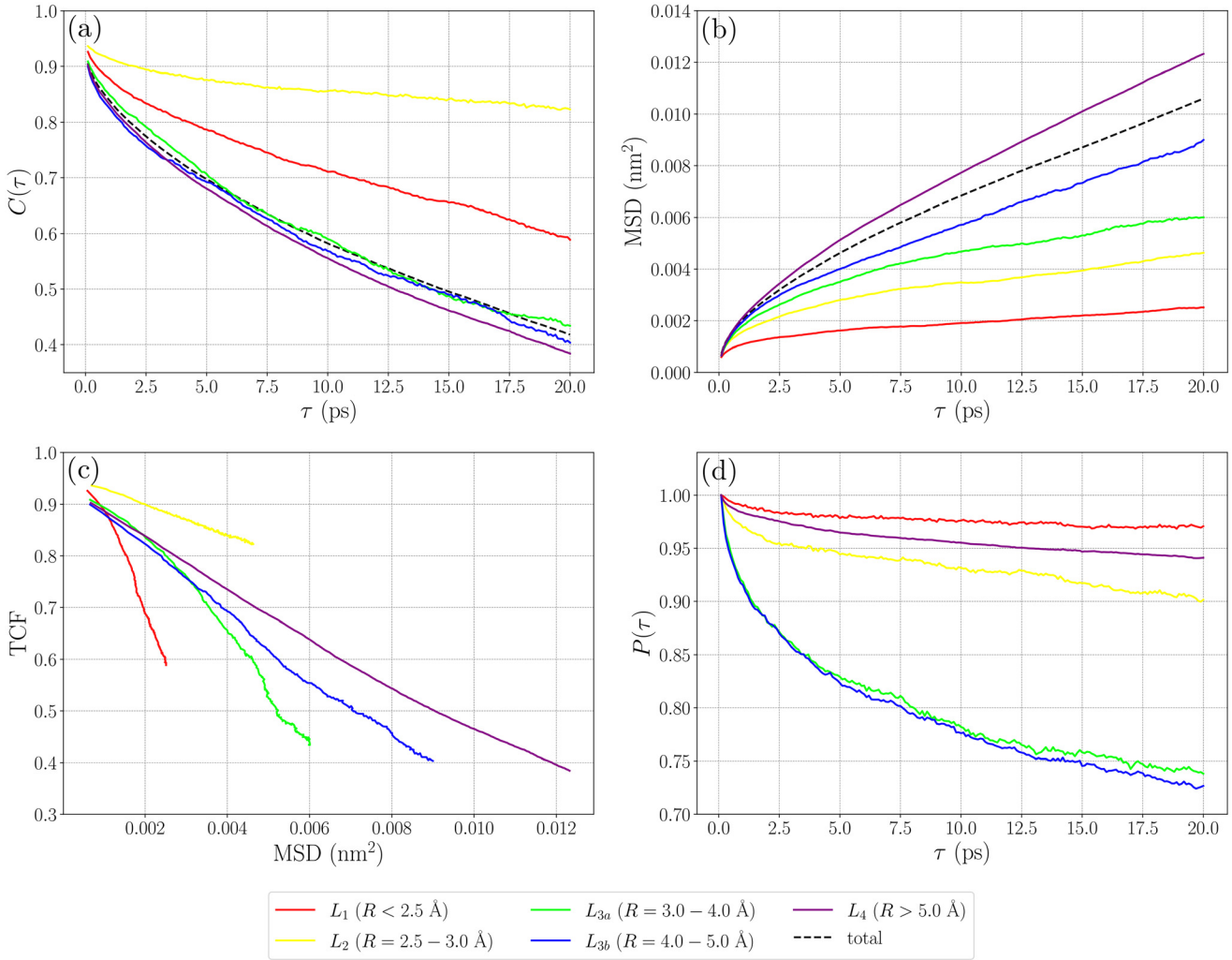

Fig. 7 (a) TCF of a second-order Legendre polynomial for O–H vectors at different distances from the nanoparticle surface, (b) MSD of oxygen atoms in water at different distances from the nanoparticle surface, (c) TCF of an OH vector as a function of MSD taken at the same time, and (d) SP for oxygen atoms in water molecules in layers located at different distances from the nanoparticle surface.

where $N(t)$ is the number of water molecules inside the region at time t and $N(t + \tau)$ is the number of water molecules remaining inside the region at a later time $t + \tau$ with τ being the lag time. The angle brackets in eqn (3) denote an average taken over all time origins t in the trajectory. While the MSD for water molecules at different distances from the nanoparticle provides information about dynamics within shells, SP provides information about diffusion between shells. We calculated the survival probability of water molecules in hydration layers L_1–L_4 and the results are shown in Fig. 7(d). It is observed that the SP for L_1 ($R < 2.5$ Å) and L_2 (2.5 Å < R < 3.0 Å) decays significantly more slowly when compared to SP for L_3 (3.0 Å < R < 5.0 Å). This shows that water molecules in the first and second hydration shells are exchanged at a very slow rate compared to water molecules further away from the surface. Comparing L_{3a} and L_{3b} (3 Å < R < 5 Å), the survival probability curves show a similar decay suggesting that inter-layer diffusion is less affected by distance to the surface beyond R = 3 Å. The high survival probability obtained for L_4 (R > 5.0 Å) is explained by the large volume of this region. It is worth pointing out that the SP for L_1 is calculated for all water molecules in this hydration layer and, therefore, water molecules undergoing adsorption/desorption at exposed edge/corner sites (see Fig. S13 in Section S7 of theESI†) can have a lower SP.

Taken together, our results indicate that both translational and rotational dynamics of water molecules substantially decrease with shorter distances to the nanoparticle surface. However, water molecules in the layer closest to the nanoparticle (L_1) undergo faster reorientation compared to those in the second hydration shell. It is possible that the extent to which these water molecules participate in hydrogen bonding is related to this effect. The decoupling of rotational and translational diffusion, where translation slows down more than rotation, is observed where water molecules in the second hydration layer (L_2) translate further per rotation compared to

water molecules in layers L_3 and L_4. Our analysis also indicates that water reorientation slows down abruptly with decreasing distance to the nanoparticle surface between shells L_3 and L_2, while a decrease of translational diffusion occurs more gradually. It can be noted that in the inner region where $R < 3$ Å (*i.e.*, L_1 and L_2), both rotational and reorientational dynamics are substantially slower compared to those in the bulk. For 3 Å $< R <$ 4 Å (*i.e.*, L_3), reorientation is as fast as in the bulk, but diffusion still occurs at a reduced rate. Analysis of survival probability in the various hydration shells showed that water molecules located within 3 Å of the surface undergo slow exchange while water molecules beyond 3 Å are replaced much more quickly.

4 Conclusion

In this work we have performed an AIMD simulation of a TiO_2-nanoparticle in water with the purpose of analyzing water structure, dynamics and reactivity on an irregular surface with curvature and edges. We have characterized the structure of the simulated TiO_2–water system using RDFs between atom types representing distinct chemical environments that were identified in the AIMD ensemble. This analysis shows that an increasing ordering of water molecules surrounding the nanoparticle persists as far out as 7–8 Å from the nanoparticle surface. Our results are in line with previous studies where the interface is described as consisting of a layer of strongly bound adsorbed water molecules and two additional layers of ordered water, one strongly bound by hydrogen bonds to bridging oxygens on the surface, and a next layer of water molecules bound by hydrogen bonds to the first two layers. In order to study surface reactivity on the TiO_2-nanoparticle surface, how the populations of different atom types change during the simulation were analyzed. We found that water molecules can dissociate at bridging oxygen sites to form hydroxyl groups and protonate the oxygen bridges. The dissociation occurs *via* a mechanism involving a proton transfer over three water molecules. One water molecule protonates the oxygen bridge, the second forms a hydroxyl group and the third water molecule transfers a proton between them. The formed hydroxyl group was found to undergo further exchange with water molecules using a similar mechanism with the proton exchange occurring through a nearby water molecule. While we observed only one of each of these effects during a 50 ps simulation, it is plausible that such reactions can occur over a few-tens of ps time scale. Furthermore, we found that water molecules at edges/corners undergo adsorption/desorption much faster than on flat surfaces, confirming these sites as being more exposed for reactions, which is of importance for catalysis. In future works we are planning to investigate further nanoparticles of varying shapes in order to understand whether these phenomena are generally observed. It can also be of interest to investigate how the mechanism for water splitting observed here is affected by including nuclear quantum effects.

We have also investigated the dynamics of water around the TiO_2-nanoparticle by calculating orientational time correlation functions and the mean square displacement of water molecules at different distances from the nanoparticle surface. We found that water reorientation rates quickly decrease at a distance of around 3 Å from the surface, while diffusion slows down more gradually when starting from longer distances. Our results also indicated that the solvation shells located 2–5 Å from the surface consist of two regions: (1) an inner region with tightly held water molecules having slow reorientational and translational dynamics; and (2) an outer region where reorientation of water molecules is as fast as in the bulk nanoparticle while diffusion occurs at a reduced rate. Overall, local atom environment analysis, and RDFs and MSDs calculated in this work give a detailed picture of the structure, dynamics and reactivity at a curved TiO_2–water interface. Furthermore, the computed water properties are important target data for parametrization and validation of classical force fields allowing for extended simulations of the aqueous interface with TiO_2-nanoparticles over much longer time and length scales.

Author contributions

F. G.: Investigation, methodology, formal analysis, visualization, writing – original draft. A. L.: conceptualization, methodology, supervision, writing – review and editing.

Conflicts of interest

There are no conflicts to declare.

Acknowledgements

This work has been supported by the Swedish Research Council (Vetenskapsrådet), grant no. 2021-04474, and by the NanoSolveIt Horizon2020 project. The computations were performed on resources provided by the Swedish National Infrastructure for omputing (SNIC) through the National Supercomputer Center (NSC, Linköping) and Center for Parallel Computing (PDC, Stockholm).

References

1 A. Afantitis, G. Melagraki, P. Isigonis, A. Tsoumanis, D. D. Varsou, E. Valsami-Jones, A. Papadiamantis, L.-J. A. Ellis, H. Sarimveis, P. Doganis, *et al.*, *Comput. Struct. Biotechnol. J.*, 2020, **18**, 583–602.
2 L. Sang, Y. Zhao and C. Burda, *Chem. Rev.*, 2014, **114**, 9283–9318.
3 F. Fang, J. Kennedy, E. Manikandan, J. Futter and A. Markwitz, *Chem. Phys. Lett.*, 2012, **521**, 86–90.
4 C. Li, C. Koenigsmann, W. Ding, B. Rudshteyn, K. R. Yang, K. P. Regan, S. J. Konezny, V. S. Batista, G. W. Brudvig,

C. A. Schmuttenmaer, *et al.*, *J. Am. Chem. Soc.*, 2015, **137**, 1520–1529.
5 F. Li, Q. Li and H. Kim, *Appl. Surf. Sci.*, 2013, **276**, 390–396.
6 A. Jaroenworaluck, W. Sunsaneeyametha, N. Kosachan and R. Stevens, *Surf. Interface Anal.*, 2006, **38**, 473–477.
7 X. Xin, M. Scheiner, M. Ye and Z. Lin, *Langmuir*, 2011, **27**, 14594–14598.
8 A. A. Kashale, K. P. Gattu, K. Ghule, V. H. Ingole, S. Dhanayat, R. Sharma, J.-Y. Chang and A. V. Ghule, *Composites, Part B*, 2016, **99**, 297–304.
9 A. Fujishima and K. Honda, *Nature*, 1972, **238**, 37–38.
10 S. Basu, A. Paul and R. Antoine, *Nanomaterials*, 2021, **12**, 62.
11 M. Amin, J. Tomko, J. J. Naddeo, R. Jimenez, D. M. Bubb, M. Steiner, J. Fitz-Gerald and S. M. O'Malley, *Appl. Surf. Sci.*, 2015, **348**, 30–37.
12 R. T. Frederick, Z. Novotny, F. P. Netzer, G. S. Herman and Z. Dohnálek, *J. Phys. Chem. B*, 2018, **122**, 640–648.
13 Y. Nam, L. Li, J. Y. Lee and O. V. Prezhdo, *J. Phys. Chem. C*, 2018, **122**, 5201–5208.
14 G. Ketteler, S. Yamamoto, H. Bluhm, K. Andersson, D. E. Starr, D. F. Ogletree, H. Ogasawara, A. Nilsson and M. Salmeron, *J. Phys. Chem. C*, 2007, **111**, 8278–8282.
15 T. Petit, J. Ren, S. Choudhury, R. Golnak, S. S. Lalithambika, M. F. Tesch, J. Xiao and E. F. Aziz, *Adv. Mater. Interfaces*, 2017, **4**, 1700755.
16 L. Zhu, Q. Gu, P. Sun, W. Chen, X. Wang and G. Xue, *ACS Appl. Mater. Interfaces*, 2013, **5**, 10352–10356.
17 Z.-T. Wang, Y.-G. Wang, R. Mu, Y. Yoon, A. Dahal, G. K. Schenter, V.-A. Glezakou, R. Rousseau, I. Lyubinetsky and Z. Dohnálek, *Proc. Natl. Acad. Sci. U. S. A.*, 2017, **114**, 1801–1805.
18 T. Zheng, C. Wu, M. Chen, Y. Zhang and P. T. Cummings, *J. Chem. Phys.*, 2016, **145**, 044702.
19 R. S. Kavathekar, P. Dev, N. J. English and J. M. D. MacElroy, *Mol. Phys.*, 2011, **109**, 1649–1656.
20 E. G. Brandt and A. P. Lyubartsev, *J. Phys. Chem. C*, 2015, **119**, 18110–18125.
21 G. Zhou, C. Liu and L. Huang, *J. Chem. Eng. Data*, 2018, **63**, 2420–2429.
22 S. Boyd, D. O'Carroll, Y. Krishnan, R. Long and N. J. English, *Crystals*, 2022, 398.
23 L. Huang, K. E. Gubbins, L. Li and X. Lu, *Langmuir*, 2014, **30**, 14832–14840.
24 M. F. C. Andrade, K. Hsin-Yu, L. Zhang, R. Car and A. Selloni, *Chem. Sci.*, 2020, **11**, 2335–2341.
25 M. E. Tuckerman, *J. Phys.: Condens. Matter*, 2002, **14**, R1297.
26 L. Agosta, E. G. Brandt and A. P. Lyubartsev, *J. Chem. Phys.*, 2017, **147**, 024704.
27 E. G. Brandt, L. Agosta and A. P. Lyubartsev, *Nanoscale*, 2016, **8**, 13385–13398.
28 L. Agosta, M. Dzugutov and K. Hermansson, *J. Chem. Phys.*, 2021, **154**, 094708.
29 I. Rouse, D. Power, E. G. Brandt, M. Schneemilch, K. Kotsis, N. Quirke, A. P. Lyubartsev and V. Lobaskin, *Phys. Chem. Chem. Phys.*, 2021, **23**, 13473–13482.
30 T. D. Kühne, M. Iannuzzi, M. Del Ben, V. V. Rybkin, P. Seewald, F. Stein, T. Laino, R. Z. Khaliullin, O. Schütt, F. Schiffmann, D. Golze, *et al.*, *J. Chem. Phys.*, 2020, **152**, 194103.
31 B. G. Lippert, J. Hutter and M. Parrinello, *Mol. Phys.*, 1997, **92**, 477–488.
32 J. VandeVondele, M. Krack, F. Mohamed, M. Parrinello, T. Chassaing and J. Hutter, *Comput. Phys. Commun.*, 2005, **167**, 103–128.
33 A. D. Becke, *Phys. Rev. A*, 1988, **38**, 3098.
34 C. Lee, W. Yang and R. G. Parr, *Phys. Rev. B: Condens. Matter Mater. Phys.*, 1988, **37**, 785.
35 S. Grimme, J. Antony, S. Ehrlich and H. Krieg, *J. Chem. Phys.*, 2010, **132**, 154104.
36 J. VandeVondele and J. Hutter, *J. Chem. Phys.*, 2007, **127**, 114105.
37 S. Goedecker, M. Teter and J. Hutter, *Phys. Rev. B: Condens. Matter Mater. Phys.*, 1996, **54**, 1703.
38 G. Bussi, D. Donadio and M. Parrinello, *J. Chem. Phys.*, 2007, **126**, 014101.
39 L. E. Walle, A. Borg, E. M. J. Johansson, S. Plogmaker, H. Rensmo, P. Uvdal and A. Sandell, *J. Phys. Chem. C*, 2011, **115**, 9545–9550.
40 M. F. C. Andrade, H.-Y. Ko, R. Car and A. Selloni, *J. Phys. Chem. Lett.*, 2018, 6716–6721.
41 T. A. Manz, *RSC Adv.*, 2017, **7**, 45552–45581.
42 D. Marx, *ChemPhysChem*, 2006, **7**, 1848–1870.